Parameterizing the Basal Melt of Tabular Icebergs

Anna FitzMaurice[a,*], Alon Stern[b]

[a] *Program in Atmospheric and Oceanic Sciences, Princeton University, Princeton, NJ*
[b] *Geophysical Fluid Dynamics Laboratory, Princeton, NJ*

Abstract

In this study, we consider the influence of icebergs on the ocean when they are modeled as occupying physical space, to answer the question of how the melting of icebergs and subsequent distribution of meltwater in the water column might be accurately parameterized in climate models. Iceberg melt is analyzed by comparing in-situ melt rates calculated via the three-equation parameterization, which was developed for application under ice shelves, with the commonly used bulk parameterization of iceberg basal melt. Our results suggest an updated velocity-independent version of the basal melt parameterization for tabular icebergs for use in calculating the basal melt rate of icebergs that are large (relative to the deformation radius), to account for the changes in ocean properties caused by the physical presence of a large iceberg in the ocean.

Keywords: icebergs, melting, meltwater, modeling, parameterization
2017 MSC:

1. Introduction

The Greenland and Antarctic ice sheets accumulate mass when snow falling on their surfaces does not melt over the course of the year, and compacts into ice over time. The ice sheets maintain equilibrium by losing mass through a combination of surface and subsurface melt, and discharging icebergs from their marine-terminating margins [1]. Recent estimates suggest that the discharge of

*Corresponding author
Email address: apf@princeton.edu (Anna FitzMaurice)

icebergs accounts for approximately half of the mass loss from the Greenland and Antarctic ice sheets [2]. From a climate modeling perspective, this mass flux to the ocean is of interest for several reasons. Firstly, the supply of meltwater to the ocean influences the properties of the water column, increasing stability if it is deposited in an almost undiluted surface layer (i.e. when there is not significant mixing with the saline ambient water as the melt plume rises to the surface), and potentially decreasing stability if it is released at depth. Increased water column stability in polar regions is associated with suppressed convection and enhanced sea ice formation, while decreased stability promotes convection and dampens sea ice growth [3, 4, 5, 6]. Secondly, enhanced nutrient availability has been observed in iceberg melt plumes, which promotes biological blooms and the sequestration of carbon by the ocean [7, 8]. There has consequently been an increased interest in understanding iceberg trajectories and melt patterns in recent years, with a to improving the representation of their influence on the ocean in global climate models.

Two different parameterizations of glacial ice melting in seawater currently exist, depending on whether the ice is attached to an ice sheet (in the form of an ice shelf) or detached from it (as an iceberg that has calved into the ocean). Within the ice shelf modeling community, the three-equation model of melt [9, 10] is used, while in the iceberg modeling community, bulk melt rate parameterizations [11, 12, 13, 14] are usually employed to circumvent the need to explicitly resolve icebergs in the ocean. However, in both scenarios it is the same physical process, namely the melting of ice in seawater, that is being represented, and thus the two parameterizations should agree.

The bulk iceberg melt parameterizations used in current global climate models account for iceberg decay via wave erosion at their margins, surface melt by the air, and subsurface melt by the ocean [15, 16, 17]. Of these, the rate of wave erosion is generally the largest, at $0.5 - 1$ m d^{-1} even in calm ocean conditions, followed by the subsurface melt (≤ 1 m d^{-1}), and then surface melt (≤ 0.02 m d^{-1}; often neglected in climate models) [17, 16]. The process of edge erosion is parametrized as a continuous decay rate (in units of m d^{-1}), and the

wave erosion rate is only applied to the iceberg sides, which generally account for a smaller area than the base. In this study, we focus on subsurface melt as opposed to edge wasting since the predominant disagreement between the representation of iceberg and ice shelf decay occurs in the parameterization of subsurface melting. Subsurface melt may further be divided into subsurface side melt and subsurface basal melt, and it is this latter process that is the focus of this study.

The bulk parameterization of iceberg basal melt (in units of m d^{-1}) is given by

$$M_b = C\frac{(T_o - T_i)|u_o - u_i|^{0.8}}{L^{0.2}}, \tag{1}$$

for ocean temperature T_o (°C), ice temperature T_i (generally taken to be constant at $T_i = -4$°C), relative ice-ocean velocity $|u_o - u_i|$ m s^{-1}, iceberg length L (m), and dimensional constant $C = 0.58$°C^{-1} $m^{0.4}$ d^{-1} $s^{0.8}$ [11, 12, 13, 16, 14]. For the bulk parameterization above, the ocean properties T_o and u_o are typically taken from a single grid cell [18, 14], although there have been recent modifications to spatially average these properties over the surface area occupied by the iceberg [19]. In the standard bulk parameterization, the surface T_o and u_o are used, although some recent models have taken the values of T_o and u_o at the basal depth [20, 21, 6, 19].

While bulk parameterizations are typically employed to represent the melting of glacial ice that is in the form of icebergs in global climate models, a different formulation of melting is generally applied to the glacial ice constituting ice shelves. This is the three-equation parameterization of melting [10], which comprises equations for the freezing point dependence on pressure and salinity, the conservation of heat, and the conservation of salt. For temperature T, salinity S, and pressure P, these may be expressed as

$$T_b = \alpha S_b + \beta + \delta P_b \tag{2}$$

$$\rho_i L_\mathrm{f} M_b = \frac{k_i^T}{h}(T_b - T_i) + \gamma_T(T_o - T_b) \tag{3}$$

$$\gamma_S(S_b - S_o) = -\rho_i S_b M_b, \tag{4}$$

	Parameter	Units
α	Freezing equation salinity coefficient	°C PSU^{-1}
β	Freezing equation constant coefficient	°C
δ	Freezing equation pressure coefficient	°C Pa^{-1}
$\rho_{i,o}$	Ice/ocean reference density	kg m^{-3}
k_i^T	Molecular salt conductivity	m^2 s^{-1}
h	Boundary layer thickness	m
γ_T	Heat turbulent transfer coefficient	W m^{-2} K^{-1}
γ_S	Salt turbulent transfer coefficient	kg m^{-2} s^{-1}

Table 1: A full explanation of the parameters in the three-equation formulation of melting (equations 3-4).

where the subscript o is used to denote far field ocean properties, b denotes boundary layer properties, and i denotes ice properties. The heat transfer coefficient γ_T is parameterized as a function of the velocity adjacent to the ice face, and the remainder of the variables are constants, defined in Table 1, and described fully in Section 4.1. In general, this parameterization is not applied to calculate iceberg melt, although in theory the same physics should apply to this problem as to the melting of sea ice and ice shelves. There have been some modeling attempts to apply the three-equation parameterization to calculate iceberg melt rates [22, 19], but to date this has been done using far-field properties, without including an iceberg with physical mass in the flow (one notable exception is [23] who model a drifting tabular iceberg submerged in the ocean using a melt parametrization which is a hybrid between the 3 equation model and the bulk parametrization).

In what follows, we use an idealized numerical model to compare the three-equation parameterization of ice shelf melt [10] and the bulk parameterization of iceberg basal melt [11], in a configuration that explicitly includes an iceberg that acts as an obstacle to the ocean flow in which it is situated. It is found that there are large discrepancies between the bulk formulation of melting and

the parameterized three-equation melt rate if the far-field flow properties are used in the bulk formulation. In addition, there is a multiplicative difference between the two parameterizations even when the appropriate basal properties are used in the bulk parameterization. We find that this difference is a result of the representation of the heat transfer coefficient differing between the two parameterizations. Consequently, an updated bulk basal melt parameterization is proposed for large tabular icebergs ($R \geq 15$ km), which estimates the basal flow properties as a function of the free flow properties, for models that do not embed icebergs physically into the ocean, and accounts for the identified multiplicative difference between the two approaches mentioned above.

The structure of this paper is as follows. The numerical model used and simulations conducted are described in Section 2, and the results of these experiments are given in Section 3. Section 4 is a discussion of the results, in which we compare the theory underlying the three-equation and bulk models of melt to reconcile these two parameterizations, and thus make recommended adaptations to the parameterization of iceberg basal melt in global climate models. Conclusions follow in Section 5.

2. Methods

2.1. Ocean Model

We consider the ocean-only Modular Ocean Model (MOM6) of the *Geophysical Fluid Dynamics Laboratory* (GFDL) [24] in an idealized configuration, at 5 km resolution. The domain is a zonally re-entrant channel in a rotating frame (Coriolis parameter $f = -1.4 \times 10^{-4}$ s^{-1}) with rigid meridional boundaries, of length $X = 1500$ km, width $Y = 1000$ km, and depth $Z = 1000$ m (Figure 1). The flow is forced by a wind stress applied to the ocean surface of the form

$$(\tau_x, \tau_y) = \Big(\tau_0 \sin\big(\frac{\pi y}{Y}\big), 0\Big), \tag{5}$$

where $\tau_0 = 0.01$ Pa in the control experiment. The model is spun up for one year from an initial stationary state with a spatially uniform temperature

field, of control value $T = 1°C$. The initial salinity field is horizontally uniform and increases linearly with depth, between $S = 32$ PSU at the surface and $S = 38$ PSU at the ocean bed. This high salinity stratification was engineered to generate a realistic open-ocean value of the Rossby deformation radius ($R_d \approx 15$ km; a value that is representative of polar oceans [25]) in the shallow model domain, which was employed for numerical tractability.

2.2. Ice Model

The iceberg is modeled using GFDL's ice shelf module [26]. This is achieved by holding the position of the iceberg fixed and considering the channel flow to be the relative velocity between the ice and the ocean, in the iceberg's frame of reference. While icebergs often drift in close agreement with the vertically averaged ocean velocity over their depth, the presence of strong wind forcing or any vertical shear in the ocean currents will result in a non-zero relative ice-ocean velocity at the iceberg base [27], and it is this relative velocity that the channel flow represents. The iceberg is positioned at $(x, y) = (250$ km, 500 km). The iceberg has a circular cross-section, with edges that slope linearly upwards over a horizontal lengthscale $L_{\text{side}} = 20$ km (Figure 1C; note that the non-smooth iceberg perimeter is a consequence of the coarseness in the model resolution). For our control simulation we use an iceberg of tabular dimensions, with basal radius $R = 20$ km and maximum draft $D = 400$ m, and internal temperature of $-10°C$. Due to the large dimensions of the iceberg, the flow beneath it should be similar to that beneath an ice shelf, and so this is an appropriate set-up in which to conduct a comparison of the three-equation parameterization of melting and the bulk parameterization of iceberg basal melt. Iceberg melt is turned off during the one-year model spin-up. Following this period, melt is parameterized by the three-equation model using the in-situ temperature, salinity, and velocity of the flow, but the iceberg shape does not evolve as the melting occurs (i.e. the melt is parameterized by fluxes in to the ocean, while the actual iceberg shape remains constant, as in [28]).

Parameter	**Control Value**	**Perturbation Range**
Domain Dimensions, (X, Y, Z)	(1500, 1000, 1) km	-
Coriolis Parameter, f	-1.4×10^{-4} s^{-1}	$f/5$ - $5f$
Maximum Wind Stress, τ_0	0.01 Pa	0 Pa - 0.025 Pa
Ocean Temperature, T_o	1°C	0°C - 5°C
Surface Salinity, $S(z = 0)$	32 PSU	-
Seabed Salinity, $S(z = -1000$ m)	38 PSU	-
Iceberg Radius, R	20 km	5 km - 50 km
Iceberg Side Slope Lengthscale, L_{side}	20 km	0 km - 20 km
Iceberg Draft, D	400 m	-
Iceberg Internal Temperature, T_i	-10°C	-10°C - 0°C

Table 2: The control and perturbation values of the numerical experiment paramters.

2.3. Numerical Experiments

A series of numerical experiments (summarized in Table 2) are performed to test how the iceberg and ice shelf parameterizations of melt compare in different parameter regimes. In these perturbation experiments we sequentially vary the flow velocity, the ocean and ice temperature, and the iceberg radius (both in absolute terms and relative to the Rossby deformation radius, $R_d \approx 15$ km in the control simulation). The purpose of this is to test the agreement between the three-equation melt rate modeled beneath the iceberg (Figure 1B), and the melt rate as predicted by the bulk melt rate parameterization (equation 1). In the bulk melt rate parameterization, M_b is a function of $|u_i - u_o|$, T_o, T_i, and L. By varying each of these terms in turn, we can assess the agreement of the two different parameterizations of melting across parameter space. In what follows, diagnostics presented are six-month averages, starting from the second month after melting was turned on, unless otherwise stated.

3. Results

3.1. Control Run

Under control conditions, there is an eddying channel flow (Figure 1A) that induces downstream cooling and freshening as the iceberg melts (Figure 1D). The presence of the iceberg submerged in the flow causes a depression of the isopycnals upstream of the iceberg (Figure 1C), as a consequence of the surface wind forcing piling up water against the upstream face of the iceberg. This induces an anticyclonic (counter-clockwise) flow around the iceberg, due to the (southern hemispheric) rotating frame, which in turn leads to the presence of a higher velocity on the southern side than the northern side of the iceberg. The melting of the iceberg, as parameterized by the three-equation model, is thus asymmetric, with a higher melt rate observed on the southern side of the iceberg than on the northern side (Figure 1B). However, the melt rate over the base of the iceberg (inner black circle in Figure 1B), which will be the focus of this study, is relatively spatially uniform. The melting of the iceberg results in downstream cooling and freshening at the surface (Figure 1D).

3.2. Perturbation Experiments

3.2.1. Varying Flow Velocity

In the first perturbation experiment, we vary the upstream (i.e. windward) flow speed by changing the value of τ_0 in equation 5, while holding the ocean temperature and internal ice temperature constant at their control values. We then calculate the in-situ basal melt rate using the three-equation parameterization, and compare this with the bulk melt rate parameterization based on the upstream ($x = 0$ km, $y = 500$ km) flow properties (Figure 2A). It is found that the melt rate is approximately constant, independent of the upstream u, contradicting the $u^{0.8}$ dependence predicted by the bulk parameterization (equation 1).

The numerical configuration employed here allows us to directly examine the basal flow properties, rather than just using the surface flow properties as

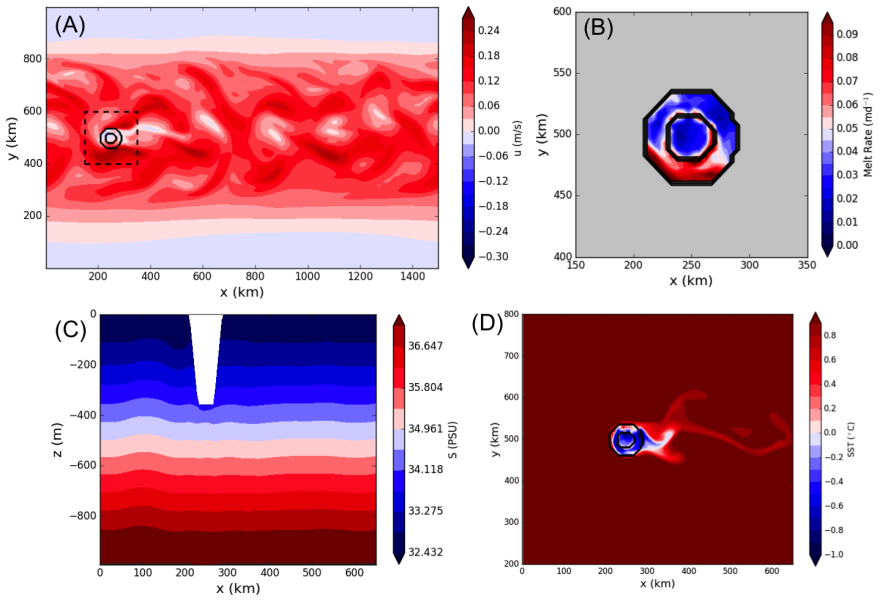

Figure 1: (A) A bird's eye snapshot of the modeled channel flow u with an iceberg of radius 20 km situated at $(x, y) = (250, 500)$ km. The inner black ring indicates the location of the flat iceberg base at depth 400 m, and the iceberg sides slope linearly upwards from this to the surface, such that the surface iceberg area is denoted by the outer black ring. The black dashed box indicates the area represented in the right-hand panel. (B) The mean melt rate over the iceberg base and sides as modeled by the three-equation parameterization. (C) A vertical snapshot of the salinity stratification, prior to melting being switched on (the iceberg is masked in white). (D) Snaphsot of the downstream SST after melting is switched on. Note that underneath the iceberg, the temperature displayed is that at the ice-ocean boundary.

proxies for these values, as is typically done when calculating iceberg basal melt using the bulk parameterization of melting. We consequently re-calculate the bulk parameterization (equation 1) using the basal flow speed and the basal temperature. We find that the three-equation melt rate collapses onto this bulk curve (Figure 2B) if two modifications are made to the standard bulk formula. Firstly, the ice temperature canonically taken to be $T_i = -4°\text{C}$ is found to be inappropriate, and instead should be replaced by the in-situ melting temperature of ice. This may be approximated beneath an iceberg (which is

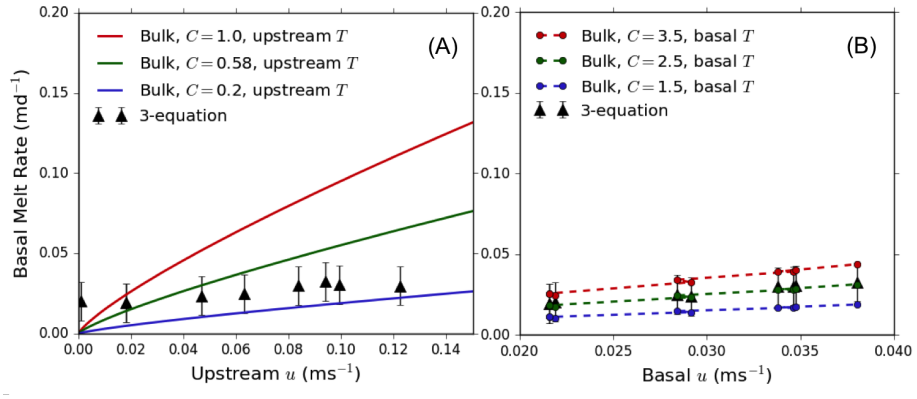

Figure 2: (A) The in-situ basal melt rate (triangles) calculated using the three-equation parameterization, plotted as a function of the model-calculated upstream flow speeds. The parameterizations of M_b as a function of speed at different C for an iceberg of radius 20 km melting in a flow at the upstream temperature are shown for reference (solid lines). (B) The in-situ basal melt rate now plotted as a function of the model-calculated basal flow speed and temperature, and the freezing temperature T_f used in place of the ice temperature T_i (dashed lines). The errorbars represent two standard deviations of the melt rate over the six-month duration of the run.

generally not at great depth) as $T_f \approx \alpha S_o + \beta$, for $\alpha = -5.73 \times 10^{-2}$°C PSU^{-1} and $\beta = 9.39 \times 10^{-2}$°C, where the upstream basal S_o may be used as an adequate first-order approximation of the basal salinity [10], and we have neglected the second-order pressure term and the higher-order salinity terms for simplicity. Secondly, the multiplicative constant in the bulk melt rate parameterization, typically taken to be $C = 0.58$ °C^{-1} m$^{0.4}$ d^{-1} s$^{0.8}$, is found to be too low, and instead the three-equation melt rate collapses onto the bulk curve

$$M_b = C\frac{(T_o - T_f)|u_o|^{0.8}}{L^{0.2}}, \tag{6}$$

for $C = 2.5$ °C^{-1} m$^{0.4}$ d^{-1} s$^{0.8}$ (Figure 2B). Here, the relative ice-ocean velocity $|u_o - u_i| = |u_o|$, as the iceberg is held fixed. The dependence of the basal flow speed on the upstream flow speed, and the multiplicative difference between the parameterizations are discussed in Section 4.

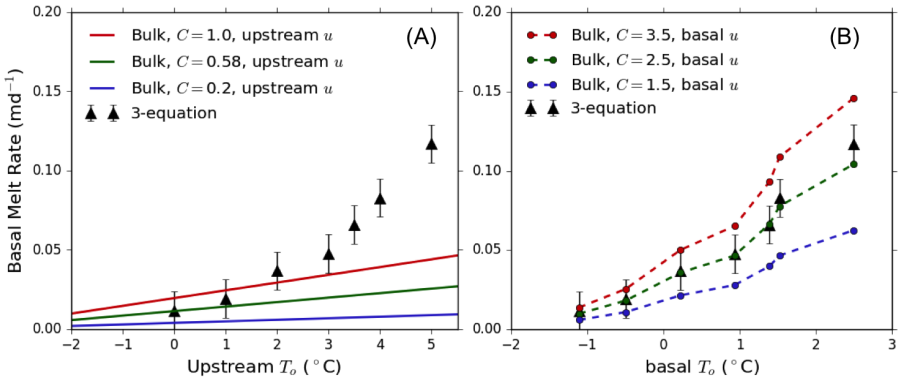

Figure 3: (A) The in-situ basal melt rate (triangles) calculated using the three-equation parameterization, plotted as a function of the upstream flow temperature. The parameterizations of M_b as a function of temperature at different C for an iceberg of radius 20 km melting in a flow at the upstream flow speed are shown for reference (solid lines). (B) The in-situ basal melt rate now plotted as a function of the model-calculated basal flow temperature, with reference curves plotted using the model-calculated basal flow speed and temperature, and the freezing temperature T_f used in place of the ice temperature T_i (dashed lines). The errorbars represent two standard deviations of the melt rate over the six-month duration of the run.

3.2.2. Varying Ocean and Ice Temperature

We next consider the influence of varying ocean temperature in the range $T_o = 0 - 4°\mathrm{C}$ on the melt rate, holding the upstream flow speed fixed at its control value. It is found that, contrary to equation 1, there is a nonlinear dependence of the basal melt rate on the upstream ocean temperature in the parameterized three-equation melt rate (Figure 3A). This nonlinear dependence of the melt rate on temperature can be attributed to an increase in the basal flow speed as T_o is increased. This is demonstrated by the fact that the three-equation melt rates collapse onto the bulk melt rate curve given by equation 6 for $C = 2.5\ °\mathrm{C}^{-1}\ \mathrm{m}^{0.4}\ \mathrm{d}^{-1}\ \mathrm{s}^{0.8}$ when the basal flow speed, as opposed to the upstream flow speed, is used in this parameterization (Figure 3B). Again, the ice temperature T_i in this parameterization has been replaced by the in-situ freezing temperature $T_f \approx \alpha S_o + \beta$.

The use of T_f rather than T_i in the bulk parameterization of basal melt is

further supported by the fact that when the ocean temperature is held fixed at $T_o = 1°\text{C}$ and the internal ice temperature is varied between -10 and $0°\text{C}$ in our numerical simulations, we find that the internal ice temperature has a negligible effect on the three-equation parameterized melt rate. The three-equation parameterization calculates the melt rate from the difference between the heat flux from the ocean to the ice-ocean boundary layer, and the heat flux from the ice-ocean boundary layer into the ice (Section 4.1). The agreement of the bulk parameterization with the three-equation parameterization of melt when T_i is replaced by T_f indicates that the contribution of the heat flux from the ice-ocean boundary layer into the ice is small, and it is the heat flux from the ocean into the ice-ocean boundary layer that dominates melting.

3.2.3. Varying Iceberg Radius

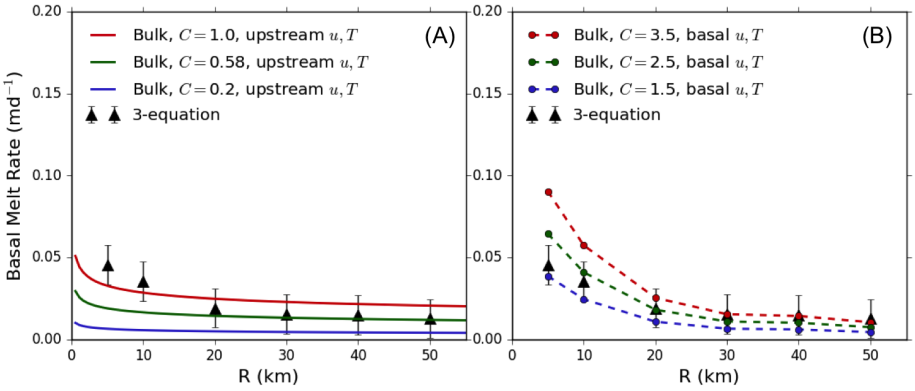

Figure 4: (A) The in-situ basal melt rate (triangles) calculated using the three-equation parameterization, plotted as a function of the iceberg radius. The parameterizations of M_b as a function of R at different C for an iceberg melting in a flow at the upstream flow speed and temperature are shown for reference (solid lines). (B) The in-situ basal melt rate again plotted as a function of the iceberg radius, but with reference curves plotted using the model-calculated basal flow speed and temperature, and the freezing temperature T_f used in place of the ice temperature T_i (dashed lines). The errorbars represent two standard deviations of the melt rate over the six-month duration of the run.

Finally, we consider varying the iceberg basal radius between 5 and 50 km, holding the free flow speed and the ocean temperature fixed at their control

values. The bulk parameterization of basal melt (equation 1) predicts a length-dependence of $L^{-0.2}$ in the melt rate, but Figure 4A illustrates that the three-equation parameterization has a stronger dependence on iceberg radius than this. If, instead, the bulk parameterization is calculated as a function of the average velocity and temperature beneath the iceberg in the numerical model, and T_i replaced with the in-situ freezing temperature T_f, the bulk parameterization is a good predictor of the in-situ melt rate for large ($R \geq R_d \approx 15$ km) icebergs, up to the previously discussed multiplicative factor of approximately 5 (Figure 4B). At small values of R, there is a smaller multiplicative difference between the two parameterizations. This point is discussed in Section 4.1.

3.2.4. Varying Ocean Stratification and Iceberg Side Slope

Although the ocean stratification and the iceberg side slope do not enter the bulk parameterization of iceberg basal melt, these properties are of interest because of their potential to influence the conditions downstream of a melting iceberg. In the perturbation experiments, we observed that the melting of the iceberg induced downstream (i.e. lee-side) cooling and freshening at the surface. It has been proposed that an iceberg melting in a cold over warm stratification might produce an increase in downstream temperature if the iceberg melt plume entrains sufficient ambient water as it rises [23].

We have not succeeded in finding a region in parameter space in which there is warming downstream of the iceberg in our numerical simulations, even in the case of a strong cold-over-warm stratification in the vertical temperature field. However, the degree to which there is downstream cooling and freshening was found to be a function of the iceberg side slope, with steeper iceberg sides resulting in a meltwater layer at the surface that is more diluted by the entrainment of ambient water. In the limiting case of vertical iceberg sides, the downstream temperature and salinity anomaly tended to zero. Given the inability of the hydrostatic numerical model considered here to explicitly simulate vertical melt plumes, the feasibility of downstream warming with a plume-resolving model would be an interesting topic of future study.

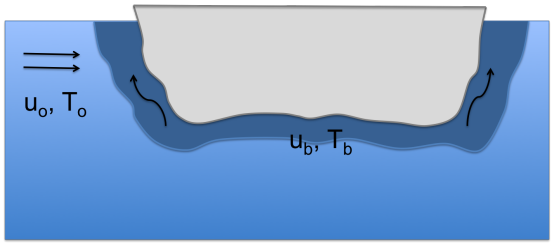

Figure 5: A schematic illustrating that it is the basal plume properties u_b, T_b that control an iceberg's melt rate, rather than the upstream free flow properties u_o, T_o.

4. Discussion

There are two main points that come out of the analysis in Sections 3.2.1-3.2.3. The first is that there is a multiplicative difference of approximately factor 5 between the bulk parameterization of iceberg basal melt and the in-situ three-equation parameterized melt rate. The second is that the upstream flow properties u_o, T_o traditionally used in the bulk parameterization to calculate the basal melt rate of icebergs are not representative of the basal flow properties in reality. Figure 5 illustrates schematically how the basal flow might be determined by the basal melt plume properties u_b, T_b, rather than the upstream flow properties. We address these two points sequentially, first comparing the theory underlying the two melt rate parameterizations in Section 4.1 to understand the origin of the multiplicative difference between them, and subsequently addressing how the basal flow properties might be predicted as a function of the upstream flow properties (which are used in this study to estimate the far-field properties traditionally used in the bulk parameterization of iceberg basal melt, as upstream in the channel is less influenced by the embedded iceberg) in Section 4.2.

4.1. Theoretical Comparison of Melt Rate Parameterizations

The parameterization of iceberg basal melt originates from the theory of heat exchange for a finite flat plate in a background flow, which has been an

extensively studied problem in engineering since the early twentieth century. The rate of heat exchange is described by the heat transfer coefficient γ_T, which has units of W m^{-2} K^{-1} and is given by

$$\gamma_T = \frac{k_o^T \bar{\mathrm{Nu}}}{L}, \tag{7}$$

where k_o^T is the thermal conductivity of the fluid (W m^{-1} °C^{-1}), L is the length of the plate (m), and $\bar{\mathrm{Nu}}$ is the average Nusselt number over the plate [11]. For a flat plate that is sufficiently long for both laminar and turbulent regimes to exist along its length, the average Nusselt number is given by

$$\bar{\mathrm{Nu}} = 0.037\ \mathrm{Re}^{0.8}\ \mathrm{Pr}^{1/3}, \tag{8}$$

where Re is the Reynold's number, and Pr is the Prandtl number of the flow [29].

In a 1973 paper, it was argued [11] that the iceberg basal melt rate could be expressed as $M_b = q/\rho_i L_\mathrm{f}$ where the heat flux is $q = \gamma_T \Delta T$ (here, ρ_i is the density of ice, L_f is the latent heat of fusion, and $\Delta T = T_o - T_i$ is the temperature difference between the ocean and the ice). The authors proceeded by using equation 8 above to substitute for γ_T, and formulated the Reynolds number of the flow as Re$= uL/\nu$, where lengthscale L is the iceberg length (m), velocity scale $u = |u_o - u_i|$ is the relative velocity between the ice and the ocean (m s^{-1}), and ν is the kinematic viscosity of water (m^2 s^{-1}). Thus,

$$\gamma_T = \frac{0.037 k_o^T \mathrm{Pr}^{1/3}}{\nu^{0.8}} \frac{u^{0.8}}{L^{0.2}}, \tag{9}$$

and hence, in units of m s^{-1},

$$M_b = \frac{\gamma_T \Delta T}{\rho_i L_f} = \Big(\frac{0.037 k_o^T \mathrm{Pr}^{1/3}}{\rho_i L_\mathrm{f} \nu^{0.8}} \Big) \frac{u^{0.8} (T_o - T_i)}{L^{0.2}} \tag{10}$$

To convert the above equation to units of m d^{-1}, a multiplicative factor of 86400 must be applied. On applying this factor and substituting for typical polar oceanic values at approximately $T_o \sim 0$°C of $k_o^T = 0.563$ W m^{-1} °C^{-1}, Pr$=$ 13.1 and $\nu = 1.826 \times 10^{-6}$ m^2 s^{-1}, equation 10 becomes the familiar

parameterization of iceberg basal melt (in units of m d^{-1});

$$M_b = 0.58 \frac{u^{0.8}(T_o - T_i)}{L^{0.2}}, \tag{11}$$

where 0.58 is a dimensional constant with units $^\circ C^{-1}$ $m^{0.4}$ d^{-1} $s^{0.8}$. Note that this constant is a composite of laboratory-derived physical constants, as opposed to being tuned to observations of icebergs melt rates.

The three-equation parameterization was developed specifically for the problem of ice melting in water. It originates from expressions for the freezing point dependence, the conservation of heat, and the conservation of salt [9, 10]. These may be written as

$$T_b = \alpha S_b + \beta + \delta P_b \tag{12}$$

$$q_i^T - q_o^T = q_{\text{latent}}^T = -\rho_i M_b L_{\text{f}} \tag{13}$$

$$q_i^S - q_o^S = q_{\text{brine}}^S = \rho_i M_b (S_i - S_b), \tag{14}$$

where ocean, boundary layer, and ice properties use subscripts o, b, and i, respectively. Here, α, β, and δ are constants, the variable q denotes fluxes of heat (superscript T) or salinity (superscript S), and L_f is again the latent heat of fusion. Note that the melt rate M_b is related to the meltwater flux w_o seen in other studies [10] by $\rho_i M_b = \rho_o w_o$. Now,

$$q_{i,o}^T = -\rho_{i,o} c_{pi,o} \kappa_{i,o}^T \frac{\partial T_{i,o}}{\partial z} = -k_{i,o}^T \frac{\partial T_{i,o}}{\partial z} \tag{15}$$

(where we have used the fact that conductivity k is related to diffusivity κ by $k = \rho c_p \kappa$), so the conservation of heat may be written as

$$-\frac{k_i^T}{h}(T_b - T_i) + k_o^T \frac{\text{Nu}}{h}(T_b - T_o) = -\rho_i M_b L_{\text{f}}. \tag{16}$$

Here, Nu allows for turbulence in the boundary layer of thickness h. The parameter

$$\gamma_T = k_o^T \frac{\text{Nu}}{h}, \tag{17}$$

is the heat transfer coefficient, and is generally parameterized as

$$\gamma_T = \frac{\rho_o c_{po} u^*}{\Gamma_t + \Gamma_m}, \tag{18}$$

where $u^* = \sqrt{c_d}u$ is the friction velocity, and the Γ's are the turbulent and molecular exchange parameters, respectively. Note that there is varied use of the parameter γ_T in the literature, with some studies defining γ_T as a heat exchange velocity (units m s^{-1}) rather than a true heat transfer coefficient (units W m^{-2} K^{-1}), and thus omitting the factor ρc_p in the equation above [10].

Substituting for the heat transfer coefficient and rearranging, equation 16 becomes

$$\rho_i L_\mathrm{f} M_b = \frac{k_i^T}{h}(T_b - T_i) + \gamma_T(T_o - T_b). \tag{19}$$

Conducting a similar analysis for the conservation of salt, and assuming that $S_i = 0$ (and thus $q_i^S = 0$) gives

$$\gamma_S(S_b - S_o) = -\rho_i S_b M_b, \tag{20}$$

where $\gamma_S = \mathrm{Nu}k_o^S/h$ represents the turbulent transfer of salt across the boundary layer, analogously to γ_T [10].

All together then, the equations become

$$T_b = \alpha S_b + \beta + \delta P_b \tag{21}$$

$$\rho_i L_\mathrm{f} M_b = \frac{k_i^T}{h}(T_b - T_i) + \gamma_T(T_o - T_b) \tag{22}$$

$$\gamma_S(S_b - S_o) = -\rho_i S_b M_b. \tag{23}$$

Note that if we assume that the ice and the boundary layer are at the same temperature and the effects of salinity are negligible, equation 22 reduces to

$$\rho_i L_\mathrm{f} M_b = \gamma_T(T_o - T_i), \tag{24}$$

which is precisely the equation $M_b = q/\rho_i L_\mathrm{f} = \gamma_T(T_o - T_i)/\rho_i L_\mathrm{f}$ used to derive the bulk melt rate.

Now it becomes clear that the two parameterizations differ primarily in their representation of the heat transfer coefficient, with

$$\gamma_{T,\mathrm{bulk}} = \frac{k_o^T \bar{\mathrm{Nu}}}{L} = \frac{k_o^T 0.037 \mathrm{Pr}^{1/3} u^{0.8}}{\nu^{0.8} L^{0.2}} \tag{25}$$

$$\gamma_{T,\mathrm{3EM}} = \frac{k_o^T \mathrm{Nu}}{h} = \frac{\rho_o c_{po} \sqrt{c_d} u}{\Gamma_t + \Gamma_m}. \tag{26}$$

The problem of reconciling the bulk and three-equation parameterizations may now be reduced to that of determining the range of validity of the two different representations of γ_T.

The bulk heat transfer coefficient $\gamma_{T,\mathrm{bulk}}$ was derived empirically from laboratory-scale flows [29], taking the Reynolds number Re$= uL/\nu$ where L is the characteristic lengthscale of the flow. For flow past a finite body, this characteristic length should be taken as the length of the body, but at some point this ceases to be the appropriate characteristic lengthscale. In the ocean, this is certainly the case when the iceberg is large relative to the Rossby deformation radius. Thus at lengthscales greater than the deformation radius, there is more reason to trust the three-equation heat transfer coefficient. Conversely, the three-equation heat transfer coefficient $\gamma_{T,\mathrm{3EM}}$ assumes fully developed thermal and turbulent boundary layers along the entire ice surface. This is not true at small lengthscales where leading edge effects are important. Thus at small lengthscales, there is more reason to trust that $\gamma_{T,\mathrm{bulk}}$ is the representative heat transfer coefficient.

In between the limiting cases of small R (laboratory scales, where $\gamma_{T,\mathrm{bulk}}$ applies) and large R (scales greater than the deformation radius, where $\gamma_{T,\mathrm{3EM}}$ applies), there should exist a matching region between the two representations of the heat transfer coefficient. An extensive exploration of basal melt rates in this parameter space using either laboratory studies or Direct Numerical Simulations (DNS) would be required to find the exact form this matching should take. One such hypothetical matching is illustrated in Figure 6.

Comparing the heat transfer coefficients, it is found that there is approximately a factor 5 difference between $\gamma_{T,\mathrm{bulk}}$ and $\gamma_{T,\mathrm{3EM}}$ in the region of parameter space covered by our numerical experiments (star in Figure 6). This goes some way towards explaining the discrepancy between the typically used value of $C = 0.58\ ^\circ\mathrm{C}^{-1}\ \mathrm{m}^{0.4}\ \mathrm{d}^{-1}\ \mathrm{s}^{0.8}$, and the value $C = 2.5\ ^\circ\mathrm{C}^{-1}\ \mathrm{m}^{0.4}\ \mathrm{d}^{-1}\ \mathrm{s}^{0.8}$ that is required for the bulk parameterization to agree with the three-equation parameterization in the numerical experiments of Section 3. For this experiment, the iceberg radius was greater than the deformation radius and thus outside

of the range of validity of the bulk parameterization heat transfer coefficient, suggesting the three-equation melt rate be trusted in this case.

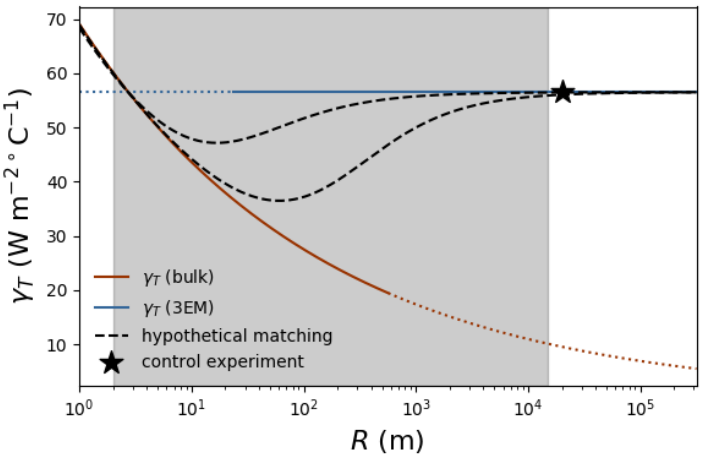

Figure 6: A comparison of the three-equation model heat transfer coefficient $\gamma_{T,\mathrm{3EM}}$ (blue line) and the bulk model heat transfer coefficient $\gamma_{T,\mathrm{bulk}}$ (red line) as a function of the iceberg radius R for a flow speed of $u = 0.02$ ms^{-1}. Note that the values of γ_T have been scaled by factor of 86400 to produce melt rates in units of m d^{-1}. At small R, $\gamma_{T,\mathrm{bulk}}$ is more physically relevant, while when R is large (certainly when $R > R_d$), $\gamma_{T,\mathrm{3EM}}$ is more physical. In between, a matching region should exist between the two heat transfer coefficients, which is approximately illustrated via the gray shading (shown extending from 2 m to $R_d = 15$ km here). Two hypothetical matchings of the form $g(R) = \frac{1}{1+cR^n}\ \gamma_{\mathrm{bulk}} + \left(1 - \frac{1}{1+cR^n}\right)\ \gamma_{\mathrm{3EM}}$, with $c = 0.005$ and 0.05, and $n = 1$, are illustrated by the black dashed lines (speculative only). The black star indicates the location in parameter space of the control numerical experiment conducted in Section 3.

4.2. Dependence of Basal Conditions on Upstream Flow Properties

Even with the correct heat transfer coefficient, the bulk melt rate parameterization requires the correct basal flow properties to be input in order for it to agree with the three-equation parameterization of the melt rate. We thus proceed by considering how the basal flow properties may be determined as a function of the upstream flow properties for the icebergs that we are interested in modeling. In the following subsections, we consider in turn the influence of

the upstream flow speed, the upstream temperature, and the iceberg radius on the basal properties (Figure 7).

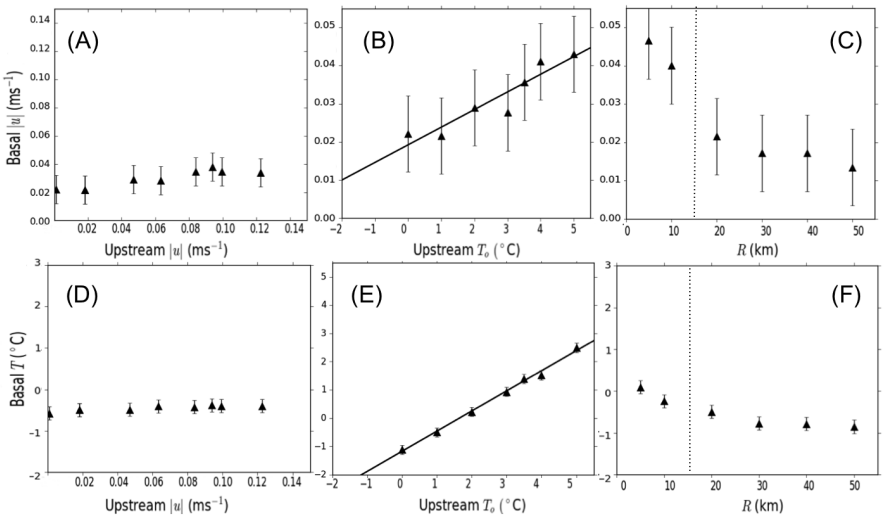

Figure 7: Top Row: The average model-calculated iceberg basal speed as a function of (A) the upstream free flow speed, (B) the upstream temperature, and (C) the iceberg radius (the vertical dashed line indicates the experimental $R_d = 15$ km). Bottom Row: The average model-calculated iceberg basal temperature as a function of (D) the upstream free flow speed, (E) the upstream temperature, and (F) the iceberg radius (the vertical dashed line indicates the experimental $R_d = 15$ km). The curves in (B) and (E) are the linear lines of best fit. They are described by the equations $u_b = 0.004T_o + 0.02$ and $T_b = 0.7T_o - 1.2$, respectively. In all panels, the errorbars represent two standard deviations of the observed quantity over the six-month duration of the run.

4.2.1. Dependence on Upstream Flow Speed

The basal flow speed is approximately independent of the upstream flow speed (Figure 7A), and the basal temperature is likewise constant at a little over a degree less than the upstream temperature (Figure 7D). Key to understanding this is the fact that even at negligible free flow speeds the ice melting causes meltwater to flow outwards under the influence of buoyancy and produce a non-zero velocity at the iceberg base. In addition, the fact that a finite-dimensional iceberg acts as an obstacle to the flow changes the relative velocity between

the ice base and the ocean. The blocking effect is enhanced by the fact that icebergs are subject to the influence of rotation, and when they become large relative to the Rossby deformation radius a Taylor column forms under the ice, reducing the relative velocity between the ice and the ocean (Figure 8). Thus in a rotating frame of reference, the velocity at the base of the ice is approximately constant at the speed of the meltwater layer.

The resultant melt rate dependence on velocity is comparable to that observed in laboratory studies of the dependence of the side melt rate of ice blocks on a background flow [30]. These experiments found that side melting is controlled by the side melt plume speed when this is higher than the background flow speed. Comparably, this study suggests that the basal melting is controlled by the basal meltwater speed when this is higher than the background flow speed (which is uniformly the case for large icebergs due to the formation of a Taylor column of reduced flow under the iceberg; see Section 4.2.3). However, the relevant velocity is now that of a horizontally spreading gravity current, as opposed to a vertical melt plume speed, so we hypothesize that it will scale as $\sqrt{g'h}$, for reduced gravity g' and meltwater layer thickness h [31].

4.2.2. Dependence on Upstream Temperature

The basal flow speed is an increasing function of the upstream temperature T_o (Figure 7B). The linear best fit to this relationship is

$$u_b = cT_o + d, \tag{27}$$

where $c = 0.004 \pm 0.003$ m s^{-1} °C^{-1} and $d = 0.02 \pm 0.01$ m s^{-1}. This agrees with the suggestion above that the basal flow speed is that of the meltwater layer, as at higher flow temperatures we would expect more melting, and thus a greater meltwater layer thickness h. We would also expect the value of the reduced gravity g' to be greater due to the increased density difference between the meltwater and the ambient water at higher ambient water temperatures. Consequently, we would expect the meltwater layer velocity $\sqrt{g'h}$ to increase with T_o.

The basal temperature is related to the upstream temperature by

$$T_b = aT_o + b, \tag{28}$$

where $a = 0.7 \pm 0.1$ is dimensionless, and $b = -1.2 \pm 0.1$ °C (line of best fit in Figure 7E). This indicates the water in contact with the iceberg base is a mixture of the ambient water at $T = T_o$ and the meltwater with $T = T_f$.

4.2.3. Dependence on Iceberg Radius

With increasing iceberg radius there is a reduction in the basal flow speed, which begins to level off at $R \approx 15$ km (Figure 7C). The reduction in the basal flow speed between $R = 5$ and $R = 15$ km relates to the formation of a Taylor column under the iceberg when as it approaches the scale of $R = 15$ km (an occurence that has previously been posited [32]). We tested the robustness of this attribution by holding the iceberg radius fixed and varying the Coriolis parameter f in our numerical simulations, and found that the same reduction in basal velocity is seen as the ratio L/R_d increases, where R_d is the Rossby radius of deformation (Figure 8D). The formation of the Taylor column can be seen in sections of the zonal velocity as the Coriolis parameter f is varied (Figure 8A-C). Once the Taylor column is fully formed, there is minimal contribution to the basal velocity from the upstream flow, and the basal $|u|$ remains constant at the speed of the meltwater layer.

In addition to the reduction in basal velocity with increasing iceberg radius, there is a reduction in the temperature at the base of the iceberg, which begins to level off at $R \approx 15$ km (Figure 7F). This may again be attributed to the formation of a Taylor column under the iceberg, as a similar pattern is produced by varying Coriolis parameter f and considering the basal temperature as a function of L/R_d (Figure 8E). Physically, the reduction in basal flow with the formation of a Taylor column may be limiting the exchange of ambient water with the water underneath the iceberg and thus resulting in a depressed basal temperature.

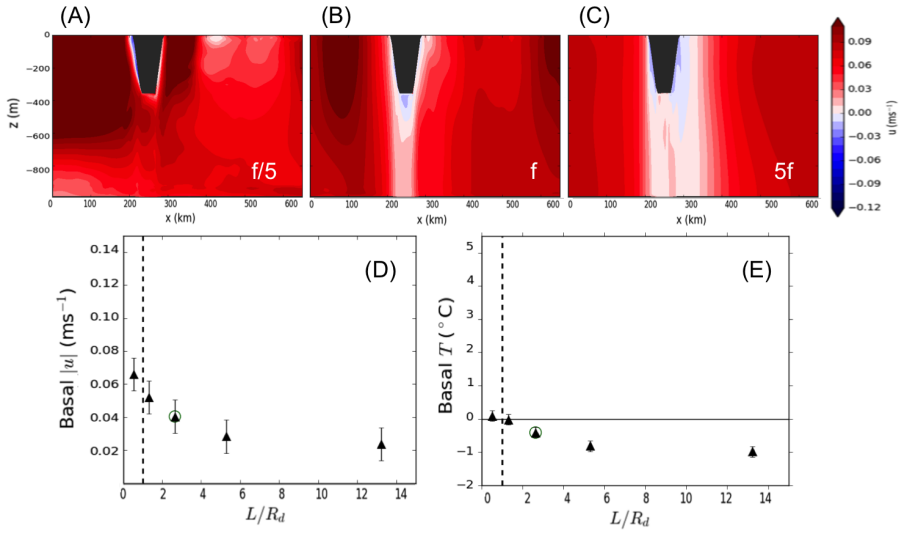

Figure 8: Row 1: Side plot of the six-month average zonal velocity field u for $f/5$, control f, $5f$. Row 2: The magnitude of the basal velocity (left) and basal temperature (right) as a function of the ratio of the iceberg lengthscale to the Rossby deformation radius L/R_d. The Rossby deformation radius R_d is 75 km, 30 km, 15 km, 8 km, and 3 km in the $f/5$, $f/2$, f, $2f$, and $5f$ runs, respectively, and the iceberg radius is held fixed at 20 km. The control run $f = -1.4 \times 10^{-4}$ s^{-1} is circled in green in both figures.

4.3. Restricting Parameter Space

We have seen that introducing an iceberg to a flow influences u_o and T_o at the ice-ocean interface. We have further argued that the bulk parameterization of basal melt is still applicable if the correct flow-adjusted u_o and T_o are used in the parameterization, the correct heat transfer coefficient is used, and the in-situ freezing point T_f is used in place of the ice temperature T_i. Over all of parameter space, the basal properties are iceberg lengthscale-dependent functions of the upstream ocean properties

$$u_b = f_L(u_o, T_o) \tag{29}$$

$$T_b = g_L(u_o, T_o), \tag{30}$$

and there is an unknown matching function between the bulk and three-equation heat transfer coefficients. So in order to parameterize iceberg basal melt without

explicitly modeling the finite-dimensional iceberg, the two-dimensional functions f and g must be known for all iceberg scales L, and the heat transfer coefficient matching function must be known.

Our lack of knowledge of the heat transfer coefficient matching function, in particular, poses a significant barrier to our ability to parameterize iceberg basal melt rates across the full range of iceberg sizes. However, parameter space can be restricted by considering the contribution to total melt from icebergs of different size classes, and limiting our attention to those icebergs that contribute the most to the total melt. Previous studies have used observed iceberg size distributions to deduce the contribution from icebergs of different size classes to the total iceberg area [33, 34]. A similar argument can be applied to show that the majority of iceberg basal melt comes from large icebergs (details in Appendix A). 80% of basal melt comes from icebergs with radii greater than 20 km, even though icebergs of this size represent less than 8 % of all icebergs, and half of all basal melt comes from icebergs with radii greater than 50 km (Figure 9). Thus, accurately representing the basal melt of large icebergs is of most importance from a modeling perspective, and we have seen that for these icebergs the three-equation heat transfer coefficient is more physical than the bulk heat transfer coefficient, and the basal properties are approximately independent of the iceberg lengthscale (Figure 7C,F).

It is important to emphasize that the above argument only provides information about the proportion of *basal* melt from icebergs of different sizes, and makes no statement about the absolute contribution of basal melt to total melt. As breaking is the dominant contributor to iceberg deterioration, and this reduces icebergs to sizes at which side melt is the main source of melting, it may indeed be the case that the total quantity of basal melt is small compared to the total quantity of side melt. However, as this paper concentrates on basal melting, the question at hand is whether basal melting is a bigger contributor from large icebergs or from small icebergs. Side erosion and side melt, rather than basal melt, are dominant for small icebergs, which means that it is less important to know the correct basal melting for small icebergs. Hence we focus

on large icebergs in this study, which is concerned solely with basal melt.

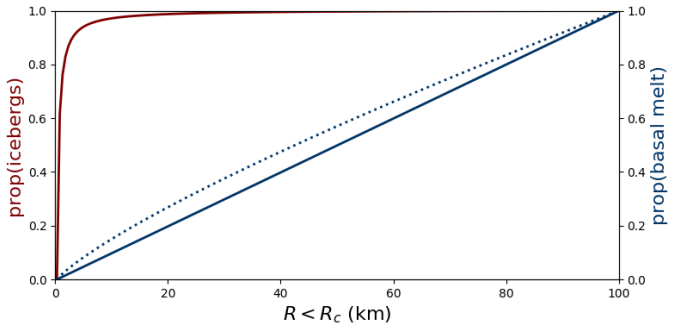

Figure 9: The cumulative density function for iceberg number (red) and iceberg basal melt (blue), as a function of iceberg radius. The solid blue line represents equation A.7, obtained if a length-independent model of melt such as the three-equation parameterization is used, and the dotted blue line represents equation A.9, obtained if the bulk parameterization of melting is used. Even though less than 8% of icebergs have radii greater than 20 km, 80% of basal melt comes from these icebergs, and 50% of basal melt comes from icebergs with radii greater than 50 km.

4.4. Proposed Melt Rate Parameterization Adaptations

Our numerical experiments have shown that the bulk melt rate parameterization agrees with the three-equation parameterization of melting up to a multiplicative factor, provided the correct basal u, T are used, and the ice temperature is replaced by the ocean freezing temperature T_f. We have argued that large (radius $R \geq R_d$) icebergs are the dominant contributors to iceberg basal meltwater, and thus accurately representing the basal melt of large icebergs is of greatest importance from a modeling perspective (the accurate representation of iceberg side melt and wave erosion is of greatest importance for small icebergs, but these deterioration mechanisms are not the focus of this study). This is especially true in the Southern Hemisphere where large tabular icebergs dominate the mass distribution. For such icebergs we have seen that the three-equation heat transfer coefficient is more physical than the bulk heat transfer coefficient. Further, for icebergs of this size, the basal flow speed is approximately constant

at the meltwater layer speed, and is independent of the relative ice-ocean velocity, represented here by the channel flow speed (as the iceberg position was held fixed). The basal temperature is related to the upstream temperature (in °C) by $T_b = 0.7T_o - 1.2$. The meltwater layer speed (m s^{-1}) is related to the upstream temperature (°C) by $u_b = 0.004T_o + 0.02$. In the Northern Hemisphere, tabular icebergs are more rare, and past models involving only smaller icebergs are likely to have greater validity.

We consequently propose the following for use in calculating the basal melt rate of large ($R \geq R_d$ km) icebergs

$$M_b = \frac{\gamma_T \Delta T}{\rho_i L_f} = \frac{\gamma_{T,\mathrm{3EM}}\big(aT_o + b - T_f\big)}{\rho_i L_f}, \tag{31}$$

where T_f is the in-situ freezing temperature, and

$$\gamma_{T,\mathrm{3EM}} = \frac{\rho_o c_{po}\sqrt{c_d}u_b}{\Gamma_t + \Gamma_m} = \frac{\rho_o c_{po}\sqrt{c_d}(cT_o + d)}{\Gamma_t + \Gamma_m}. \tag{32}$$

Here, the heat transfer coefficient has been expressed as a function of the basal flow speed, which is given by $u_b = cT_o + d$. Note that a factor of 86400 would need to be applied to this expression to produce a melt rate in units of m d^{-1} (as opposed to m s^{-1}). From the lines of best fit in Figure 7, $a = 0.7 \pm 0.1$ (dimensionless), $b = -1.2 \pm 0.1$ °C, $c = 0.004 \pm 0.003$ m s^{-1} °C^{-1}, and $d = 0.02 \pm 0.01$ m s^{-1} (equations 27-28).

For icebergs that are large relative to the deformation radius, this parameterization agrees more closely with the three-equation parameterization of basal melt than the commonly used bulk parameterization (Figure 10), particularly as the relative ice-ocean velocity or the ocean temperature become large. In these regimes, the old parameterization may overestimate the basal melt rate by factor ~ 2 when $|u_o - u_i| \approx 0.1$ m s^{-1}, or underestimate the basal melt rate by factor ~ 5 when $T_o \approx 5$°C.

While icebergs that are smaller than the deformation radius are estimated to contribute less than 20% of iceberg basal melt to the ocean, significant challenges remain if we do wish to accurately parameterize their basal melting (an important endeavor, as all icebergs will, at some stage in their lifespan, exist in

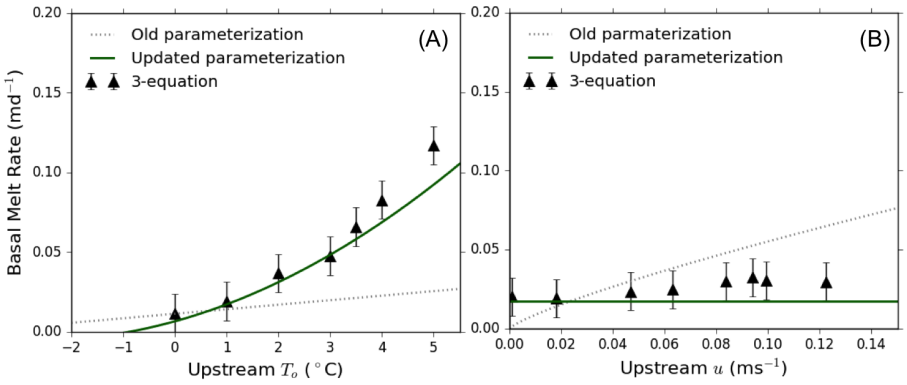

Figure 10: A comparison of the updated parameterization of tabular iceberg basal melt (equation 31, green solid lines) to the old bulk parameterization of basal melt (equation 6, gray dotted lines) and the in-situ melt rate calculated using the three-equation parameterization of melt (black triangles, errorbars representing two standard deviations of the observed quantity over the six-month duration of the run), (A) as the upstream flow speed u is varied, and (B) as the upstream temperature T_o is varied. This parameterization is proposed for use with icebergs that are large relative to the deformation radius.

this size class). It is not be appropriate to use the three-equation parameterization at small scales because the turbulence beneath the iceberg is not fully developed. Instead, modifications must be made to the bulk parameterization of melting.

Firstly, it is unclear what form the heat transfer coefficient should take if these icebergs are larger than laboratory dimensions. It is reasonable to assume that some matching exists between the laboratory-scale bulk heat transfer coefficient and the large-scale three-equation heat transfer coefficient (Figure 6), but further studies are needed to determine the form of this matching. Secondly, even if the heat transfer coefficient were known, the basal flow properties are lengthscale-dependent functions of the upstream flow properties for small ($R < R_d$) icebergs. Thus for each iceberg lengthscale below the deformation radius, both the heat transfer coefficient and the dependence of the basal flow properties on the upstream flow properties must be found in order to parameterize the basal melt rate.

5. Conclusions

In this paper we address the fact that there are currently two different parameterizations to represent the melting of ice used in the different communities of ice shelf and iceberg modelers, respectively. The former community uses the temperature, salinity, and velocity fields adjacent to the ice to determine melt rates, and these fields respond to the injection of meltwater as melting occurs. The latter community relies on bulk parameterizations based on the flow properties that are unaffected by the presence of a melting iceberg, in essence as though the iceberg were levitating above the ocean. These two parameterizations represent the same physical process, namely the melting of ice, and as such should agree across parameter space.

By introducing an iceberg to an idealized re-entrant channel flow using GFDL's ice shelf model, we directly compared the melt parameterized using the three-equation parameterization to that predicted by the bulk parameterization of melt using the upstream flow properties (i.e. the flow unmodified by the physical presence of the iceberg). It was found that there are three sources of discrepancy between the two parameterizations. Firstly, the upstream flow properties are not representative of the basal flow properties when an iceberg occupying physical space is introduced to the flow, and thus the bulk parameterization of basal melt diverges from the three-equation parameterization of melt if the correct basal properties are not used. Secondly, even when the correct basal u and T are applied in the bulk parameterization of melt, there is approximately a factor 5 difference between this and the three-equation parameterization of melt for an iceberg of the control dimensions. Thirdly, the temperature that governs the rate of heat flux from the ocean to the ice is the in-situ freezing temperature T_f, rather than the internal ice temperature.

To understand the discrepancy between the melt parameterizations, we returned to the theoretical formulation of the two parameterizations and found that they differ in their representations of the heat transfer coefficient γ_T. We argued that the use of a Reynolds number based on the lengthscale of the iceberg

in the bulk parameterization of melt is inappropriate for tabular icebergs, given their large scale ($R \geq 15$ km), and that this leads to the observed multiplicative difference between the heat transfer coefficients in the two parameterizations. Conversely, the use of the three-equation heat transfer coefficient would be unphysical at small iceberg scales, for which the thermal and turbulent boundary layers are not fully formed over the majority of the ice length, and leading edge effects are still important to the mean melt rate. A matching between the two representations of the heat transfer coefficient is required at intermediate scales, and remains an important topic of future study.

In the absence of a known matching between the heat transfer coefficients, we proceeded by restricting our consideration to large icebergs ($R > R_d$), which we showed probabilistically to be the dominant contributers of iceberg basal melt to the ocean (although it is worth noting that iceberg basal melt is likely not the dominant contributor to *total* iceberg melt). Due to the formation of a Taylor column under such icebergs, we found that the basal flow speed was approximately independent of the upstream flow speed, and instead was simply a linear function of the ambient water temperature. The basal temperature was likewise a linear function of the upstream temperature. We thus propose an updated parameterization to calculate the basal melt rate of tabular icebergs with $R > R_d$ (equation 31), which is independent of the upstream flow speed, and which is based on the (more physical at this scale) three-equation heat transfer coefficient.

Finally we noted that there is downstream cooling and freshening at the surface associated with the melting of an iceberg with physical size in these numerical runs. However, the degree to which this cooling and freshening occurs is a function of the iceberg side slope, with the downstream SST and SSS anomalies tending to zero as the iceberg slope becomes infinite. This leaves reason to suppose that downstream warming may have been possible if the model had explicitly resolved vertical, entraining melt plumes.

Past efforts to model icebergs in GCMs have focused on smaller icebergs because of the numerical difficulties involved in modeling larger tabular icebergs.

However, recent studies have highlighted the importance of modeling larger icebergs, especially in the Southern Hemisphere, and there has consequently been an effort towards including larger icebergs in GCMs. The results presented in this study suggest that the melt rate formulations used for small icebergs are not appropriate for these larger icebergs. This paper suggests an alternative parametrization that can be used when representing large tabular icebergs as point particles.

Appendix A. The Contribution to Total Iceberg Melt from Icebergs of Different Sizes

The probability density function for icebergs of area A is given by

$$p_A(A) \propto A^{-\frac{3}{2}}, \tag{A.1}$$

for $A \in (A_-, A_+) = (10^{-1}, 10^4)$ km^2 [33]. We would like to use this distribution to estimate the proportion of basal melt that comes from icebergs of different radii. We start by changing variables from iceberg area A to iceberg radius R using the change of variables formula for probability density functions

$$p_R(R) = |\frac{\mathrm{d}}{\mathrm{d}R}\big(f^{-1}(R)\big)|\; p_A\big(f^{-1}(R)\big), \tag{A.2}$$

where $R = f(A) = A^{1/2}$. This gives a probability density function for icebergs of radius R of

$$p_R(R) = p_0 R^{-2}. \tag{A.3}$$

Here, $R \in (R_-, R_+) = (10^{-1/2}, 10^2)$ km, and the constant p_0 is chosen as $p_0 = \big(\frac{1}{R_-} - \frac{1}{R_+}\big)^{-1}$, to ensure that the probability density function p_R integrates to 1 over this range. The proportion of icebergs with radius less than any given value R_C is then given by the integral

$$\begin{aligned} \mathrm{prop(icebergs, R < R_C)} &= \textstyle\int_{R_-}^{R_C} \; p_0 R^{-2}\; \mathrm{d}R & \text{(A.4)} \\ &= p_0\big(\tfrac{1}{R_-} - \tfrac{1}{R_C}\big). & \text{(A.5)} \end{aligned}$$

If we assume that the basal melt flux is proportional to the iceberg basal area, the proportion of *basal melt* coming from icebergs with radius less than a given value R_C is given by the area-weighted integral

$$\begin{aligned} \text{prop}(\text{melt}, \text{R} < \text{R}_\text{C}) &= \int_{R_-}^{R_C} p_1 R^{-2} R^2 \, \text{d}R, & \text{(A.6)} \\ &= p_1 \big(R_C - R_-\big), & \text{(A.7)} \end{aligned}$$

where the constant $p_1 = \big(R_+ - R_-\big)^{-1}$ to ensure that the probability density function $p_1 R^{-2} R^2$ integrates to 1 over the range of the distribution $R \in (R_-, R_+)$. This is modified to

$$\begin{aligned} \text{prop}(\text{melt}, \text{R} < \text{R}_\text{C}) &= \int_{R_-}^{R_C} p_2 R^{-2} R^{1.8} \, \text{d}R, & \text{(A.8)} \\ &= \tfrac{p_2}{0.8} \big(R_C^{0.8} - R_-^{0.8}\big). & \text{(A.9)} \end{aligned}$$

if we assume that the basal melt flux is inversely proportional to $R^{0.2}$, as in the bulk parameterization of basal melt. Again, $p_2 = 0.8\big(R_+^{0.8} - R_-^{0.8}\big)^{-1}$ so that $p_2 R^{-2} R^{1.8}$ integrates to 1 over (R_-, R_+). In fact, the difference between the two parameterizations on the proportion of basal melt coming from icebergs of different sizes is minimal, and the majority of basal melt comes from large icebergs, despite these representing a small proportion of the total *number* of icebergs (Figure 9).

If we follow a single iceberg through time, it will predominantly deteriorate through breaking until it reaches small scales, at which point side melting and wave erosion will become the dominant deterioration mechanisms. However, the distribution of iceberg sizes presented above [33] is a steady state distribution. It is thus equally true to say that at *any given time*, this distribution can be used to infer a snapshot of the proportion of melt coming from icebergs of any given size class, and these proportions remain static over time.

The important caveat to this argument is that it only provides information about the proportion of *basal* melt from icebergs of different sizes, not about the contribution of basal melt to total melt. If icebergs generally break down to small scales before melting by side melting and wave erosion, then the proportion of total melt accounted for by basal melting, and thus the proportion of

total melt from tabular icebergs, will be small. However, within the remit of this study, which focuses exclusively on the parameterization of iceberg basal melting, it is accurate to state that tabular icebergs are the dominant contributors, and thus restrict our consideration to these icebergs.

Acknowledgments

The authors thank A. Adcroft, M. Bushuk, and C. Cendese for helpful discussions and comments on the manuscript. A.F. was supported by NA14OAR4320106 from the National Oceanic and Atmospheric Administration, U.S. Department of Commerce. The statements, findings, conclusions, and recommendations are those of the authors and do not necessarily reflect the views of the National Oceanic and Atmospheric Administration, or the U.S. Department of Commerce.

References

References

[1] E. Hanna, F. J. Navarro, F. Pattyn, C. M. Domingues, X. Fettweis, E. R. Ivins, R. J. Nicholls, C. Ritz, B. Smith, S. Tulaczyk, et al., Ice-sheet mass balance and climate change, Nature 498 (7452) (2013) 51.

[2] M. A. Depoorter, J. Bamber, J. Griggs, J. Lenaerts, S. R. Ligtenberg, M. Van den Broeke, G. Moholdt, Calving fluxes and basal melt rates of antarctic ice shelves, Nature 502 (7469) (2013) 89.

[3] H. G. Gade, When ice melts in sea water: A review, Atmosphere-Ocean 31 (1) (1993) 139–165.

[4] G. R. Stephenson, J. Sprintall, S. T. Gille, M. Vernet, J. J. Helly, R. S. Kaufmann, Subsurface melting of a free-floating antarctic iceberg, Deep Sea Research Part II: Topical Studies in Oceanography 58 (11) (2011) 1336–1345.

[5] J. J. Helly, R. S. Kaufmann, G. R. Stephenson, M. Vernet, Cooling, dilution and mixing of ocean water by free-drifting icebergs in the weddell sea, Deep Sea Research Part II: Topical Studies in Oceanography 58 (11) (2011) 1346–1363.

[6] N. Merino, J. Le Sommer, G. Durand, N. C. Jourdain, G. Madec, P. Mathiot, J. Tournadre, Antarctic icebergs melt over the southern ocean: Climatology and impact on sea ice, Ocean Modelling 104 (2016) 99–110.

[7] K. L. Smith, B. H. Robison, J. J. Helly, R. S. Kaufmann, H. A. Ruhl, T. J. Shaw, B. S. Twining, M. Vernet, Free-drifting icebergs: hot spots of chemical and biological enrichment in the weddell sea, science 317 (5837) (2007) 478–482.

[8] L. P. Duprat, G. R. Bigg, D. J. Wilton, Enhanced southern ocean marine productivity due to fertilization by giant icebergs, Nature Geoscience 9 (3) (2016) 219–221.

[9] M. G. McPhee, G. A. Maykut, J. H. Morison, Dynamics and thermodynamics of the ice/upper ocean system in the marginal ice zone of the greenland sea, Journal of Geophysical Research: Oceans 92 (C7) (1987) 7017–7031.

[10] D. M. Holland, A. Jenkins, Modeling thermodynamic ice–ocean interactions at the base of an ice shelf, Journal of Physical Oceanography 29 (8) (1999) 1787–1800.

[11] W. F. Weeks, W. Campbell, Icebergs as a fresh-water source: an appraisal, Journal of Glaciology 12 (65) (1973) 207–233.

[12] G. R. Bigg, M. R. Wadley, D. P. Stevens, J. A. Johnson, Prediction of iceberg trajectories for the north atlantic and arctic oceans, Geophysical research letters 23 (24) (1996) 3587–3590.

[13] R. M. Gladstone, G. R. Bigg, K. W. Nicholls, Iceberg trajectory modeling and meltwater injection in the southern ocean, Journal of Geophysical Research: Oceans 106 (C9) (2001) 19903–19915.

[14] T. Martin, A. Adcroft, Parameterizing the fresh-water flux from land ice to ocean with interactive icebergs in a coupled climate model, Ocean Modelling 34 (3) (2010) 111–124.

[15] M. El-Tahan, S. Venkatesh, H. El-Tahan, Validation and quantitative assessment of the deterioration mechanisms of arctic icebergs, Journal of Offshore Mechanics and Arctic Engineering 109 (1) (1987) 102–108.

[16] S. Savage, Aspects of iceberg deterioration and drift, Geomorphological Fluid Mechanics (2001) 279–318.

[17] G. Bigg, Icebergs: their science and links to global change, Cambridge University Press, 2016.

[18] I. Kubat, M. Sayed, S. B. Savage, T. Carrieres, G. Crocker, et al., An operational iceberg deterioration model, in: The Seventeenth International Offshore and Polar Engineering Conference, International Society of Offshore and Polar Engineers, 2007.

[19] T. Rackow, C. Wesche, R. Timmermann, H. H. Hellmer, S. Juricke, T. Jung, A simulation of small to giant antarctic iceberg evolution: Differential impact on climatology estimates, Journal of Geophysical Research: Oceans 122 (4) (2017) 3170–3190.

[20] T. Silva, G. Bigg, K. Nicholls, Contribution of giant icebergs to the southern ocean freshwater flux, Journal of Geophysical Research: Oceans 111 (C3) (2006) C03004.

[21] R. Marsh, V. Ivchenko, N. Skliris, S. Alderson, G. R. Bigg, G. Madec, A. T. Blaker, Y. Aksenov, B. Sinha, A. C. Coward, et al., Nemo–icb (v1. 0): interactive icebergs in the nemo ocean model globally configured at eddy-permitting resolution, Geoscientific Model Development 8 (5) (2015) 1547–1562.

[22] D. Jansen, M. Schodlok, W. Rack, Basal melting of a-38b: A physical model constrained by satellite observations, Remote Sensing of Environment 111 (2-3) (2007) 195–203.

[23] A. Stern, A. Adcroft, O. Sergienko, G. Marques, Modeling tabular icebergs submerged in the ocean, Journal of Advances in Modeling Earth Systems (9) (2017) 1948–1972.

[24] R. Hallberg, A. Adcroft, J. P. Dunne, J. P. Krasting, R. J. Stouffer, Sensitivity of twenty-first-century global-mean steric sea level rise to ocean model formulation, Journal of Climate 26 (9) (2013) 2947–2956.

[25] D. B. Chelton, R. A. Deszoeke, M. G. Schlax, K. El Naggar, N. Siwertz, Geographical variability of the first baroclinic rossby radius of deformation, Journal of Physical Oceanography 28 (3) (1998) 433–460.

[26] D. Goldberg, C. Little, O. Sergienko, A. Gnanadesikan, R. Hallberg, M. Oppenheimer, Investigation of land ice-ocean interaction with a fully coupled ice-ocean model: 1. model description and behavior, Journal of Geophysical Research: Earth Surface 117 (F2) (2012) 2037.

[27] A. FitzMaurice, F. Straneo, C. Cenedese, M. Andres, Effect of a sheared flow on iceberg motion and melting, Geophysical Research Letters 43 (24).

[28] X. S. Asay-Davis, S. L. Cornford, B. K. Galton-Fenzi, R. M. Gladstone, G. H. Gudmundsson, D. M. Holland, P. R. Holland, D. F. Martin, Experimental design for three interrelated marine ice sheet and ocean model intercomparison projects: Mismip v. 3 (mismip+), isomip v. 2 (isomip+) and misomip v. 1 (misomip1), Geoscientific Model Development 9 (7) (2016) 2471.

[29] E. Eckert, R. Drake, Heat and Mass Transfer, McGraw, 1959.

[30] A. FitzMaurice, C. Cenedese, F. Straneo, Nonlinear response of iceberg side melting to ocean currents, Geophysical Research Letters 44 (11) (2017) 5637–5644.

[31] G. K. Vallis, Atmospheric and oceanic fluid dynamics, Cambridge University Press, 2017.

[32] M. Crepon, M. Houssais, B. S. Guily, The drift of icebergs under wind action, Journal of Geophysical Research: Oceans 93 (C4) (1988) 3608–3612.

[33] J. Tournadre, N. Bouhier, F. Girard-Ardhuin, F. Rémy, Antarctic icebergs distributions 1992–2014, Journal of Geophysical Research: Oceans 121 (1) (2016) 327–349.

[34] A. Stern, A. Adcroft, O. Sergienko, The effects of antarctic iceberg calving-size distribution in a global climate model, Journal of Geophysical Research: Oceans 121 (8) (2016) 5773–5788.